Universal Entanglement of Typical States in Constrained Systems

S. C. Morampudi, A. Chandran, and C. R. Laumann
Department of Physics, Boston University, Boston, Massachusetts 02215, USA

(Received 19 October 2018; revised manuscript received 30 April 2019; accepted 5 December 2019; published 6 February 2020)

Constraints play an important role in the entanglement dynamics of many quantum systems. We develop a diagrammatic formalism to exactly evaluate the entanglement spectrum of random pure states in large constrained Hilbert spaces. The resulting spectra may be classified into universal "phases" depending on their singularities. The simplest class of local constraints reveals a nontrivial phase diagram with a Marchenko-Pastur phase which terminates in a critical point with new singularities. We propose a certain quantum defect chain as a microscopic realization of the critical point. The much studied Rydberg-blockaded or Fibonacci chain lies in the Marchenko-Pastur phase with a modified Page correction to the entanglement entropy. Our results predict the entanglement of infinite temperature eigenstates in thermalizing constrained Floquet spin chains, as we confirm numerically.

DOI: 10.1103/PhysRevLett.124.050602

Consider a bipartition of a random pure state $|\psi\rangle$ into two equal subsystems. The entanglement across the cut is captured by the density of states (DOS) of the reduced density matrix $\hat{\rho}$ [1]. Random matrix theory, which is widely used to describe statistical properties of quantum chaotic systems [2–6], predicts that the DOS is given by the Marchenko-Pastur (MP) distribution [7],

$$p_{\mathrm{MP}}(\epsilon) = \frac{1}{2\pi}\sqrt{\frac{4-\epsilon}{\epsilon}} \quad \text{for } \epsilon \in (0,4). \tag{1}$$

The connection to quantum chaos is provided by the hypothesis that eigenstates and late-time states at infinite temperature are indistinguishable from random pure states within subsystems [8–15]. One consequence is the widely observed Page correction [16] to the entanglement entropy of eigenstates [17–21].

Many physical systems inhabit constrained Hilbert spaces as a consequence of either global symmetries or local energetic constraints. The latter include frustrated magnets [22,23], pinned non-Abelian anyons [24,25] and ultracold Rydberg ensembles [26,27]. Recent measurements of entanglement [28] and quench dynamics in Rydberg-blockaded chains [27] raise questions about the structure of entanglement in constrained spaces [29–33]. The lack of tensor product structure implies that even the reduced density matrix of the infinite temperature mixed state $\hat{\rho}^{T=\infty}$ need not be a simple identity. We compute exactly the entanglement DOS $p(\epsilon)$ and the Page corrections of random pure states for a wide array of locally and globally constrained Hilbert spaces and find that $p(\epsilon)$ generically deviates from the MP law Eq. (1).

We find that the entanglement distribution $p(\epsilon)$ is "universal" in two senses. First, for a given constrained space, we expect $p(\epsilon)$ to describe the entanglement of eigenstates and late-time states at infinite temperature of *any* quantum chaotic Hamiltonian. We numerically confirm this for several models. Second, $p(\epsilon)$ can be grouped into "entanglement phases" as a function of the constraint parameters according to their singularities at small ϵ. Figure 1 shows an example phase diagram. Remarkably,

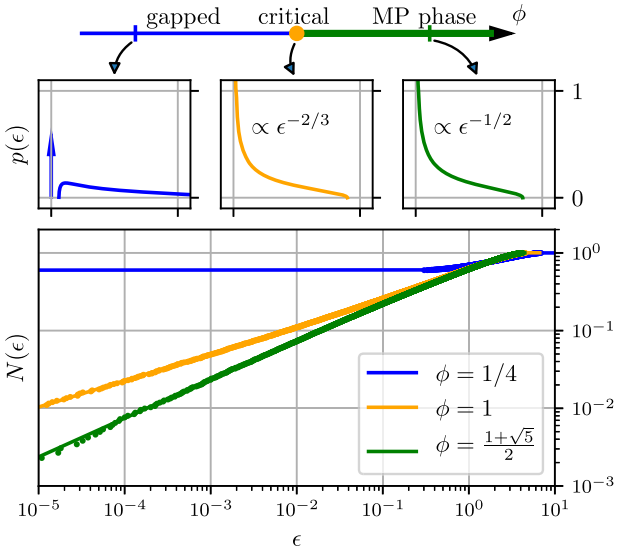

FIG. 1. Evolution of the entanglement DOS $p(\epsilon)$ as a function of the relative dimension ϕ of the sectors $l = 0, 1$. The critical divergence $p \sim \epsilon^{-1/2}$ persists through the MP phase ($\phi > \phi_c = 1$, green). This gives way to a gapped spectrum with a finite weight delta function at $\epsilon = 0$ ($\phi < 1$, blue) across a multicritical point ($\phi = 1$, orange) with distinct critical exponents, $p \sim \epsilon^{-2/3}$. (bottom) Integrated density of states $N(\epsilon)$ at three representative values, including the Rydberg or Fibonacci chain at $\phi = (1+\sqrt{5})/2$, and the defect chain at $\phi = 1$. Solid lines are analytic forms with numerical data from the diagonalization of an $N = 1000$ random pure state overlaid (points).

 © 2020 American Physical Society

the $\epsilon^{-1/2}$ singularity of the MP distribution in unconstrained spaces is stable to the addition of constraints. This MP *phase* ends at an exotic critical point where the singularity is modified to $\epsilon^{-2/3}$.

Our exact technique represents $p(\epsilon)$ in terms of diagrams which become planar in the thermodynamic limit. The constraints dress the diagrams with nontrivial "spin" structure which fortunately still admits a resummation. Below, we discuss how to parametrize constrained Hilbert spaces, before turning to the general diagrammatic method. We then solve for the entanglement DOS in two cases. First, we consider a locally constrained family of models, derive Fig. 1, and confirm our analytic predictions in Floquet quasienergy states. For the special case of the Rydberg chain, we compute the Page corrections to the von Neumann entropy. Second, we consider systems with global conservation laws—these produce diagonal constraints. We close with general comments on entanglement phases and the Page correction.

Parametrizing constrained spaces.—Consider a length $2L$ chain partitioned into two equal halves. The states of the left half can be grouped into sectors labeled by l with Hilbert space dimension Nd_l. Typically, N scales exponentially with L while the relative dimension d_l remains finite as $L \to \infty$. Similarly, each sector r of the right half has dimension Nd'_r.

Constraints may impose that certain combinations of (l, r) are disallowed in the global Hilbert space. We parametrize such constraints by a matrix C with $C_{lr} = 1$ if lr is allowed and 0 otherwise. As we will see, at large N, the entanglement of a random pure state depends only on the constraint matrix C_{lr} and the relative dimension vectors d_l, d'_r of the sectors. Note that $C = (1)$, $d = d' = (1)$ in unconstrained systems.

Our primary example of a locally constrained system is a "blockaded" chain (see Fig. 2). Each site of the chain may be in state 0 or 1 with l, r corresponding to the state of the Lth and $(L+1)$th sites on either side of the cut. The blockade disallows the $(l, r) = (1, 1)$ sector:

$$C = \begin{pmatrix} 1 & 1 \\ 1 & 0 \end{pmatrix}, \qquad d = d' = \begin{pmatrix} \phi \\ 1 \end{pmatrix}, \tag{2}$$

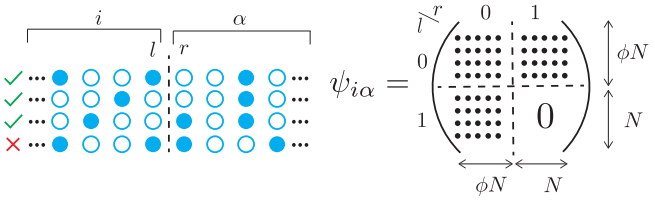

FIG. 2. (left) Configurations of a blockaded chain. The bottom configuration is disallowed by the constraint. The multi-indices i and α label configurations in the left and right subsystems, while l, r label the states of the boundary sites. (right) Block structure of a pure state. The constraints impose that the (1,1) block is zero.

where $\phi \equiv d_0/d_1$ depends on the structure of the Hilbert space away from the cut. Much of the discussion below is general in terms of C, d, and d'; we specialize formulas to the blockaded chain using $\triangleq$.

The blockaded Hilbert space arises naturally in certain Rydberg atom experiments [27], dimer ladders [31], pinned Fibonacci anyon chains [24,25], and defect chains [34]. For example, in atomic Rydberg chains, the 0 and 1 states correspond to the ground and excited states of each atom; Rydberg blockade imposes that no two consecutive atoms are excited. This rule leads to the relative dimension $\phi = (1+\sqrt{5})/2$ with $N \sim \phi^L$. If, on the other hand, the blockade is only active across the central cut due to a strong bond "defect," then $\phi = 1$ and $N \sim 2^L$. See Supplemental Material [34] for more details and models realizing other values of ϕ.

Constrained diagrams.—Let $|\psi\rangle$ be a Gaussian random pure state normalized such that

$$\overline{\psi_{i\alpha}\psi^\dagger_{\beta j}} = \frac{1}{N}\delta_{i\alpha,j\beta} = \frac{1}{N}\sum_{l,r} C_{lr}\delta^l_{ij}\delta^r_{\alpha\beta}$$
$$\triangleq \frac{1}{N}(\delta^0_{ij}\delta^0_{\alpha\beta} + \delta^1_{ij}\delta^0_{\alpha\beta} + \delta^0_{ij}\delta^1_{\alpha\beta}). \tag{3}$$

Here, $\psi^\dagger_{\beta j} = \psi^*_{j\beta}$ is the conjugate transpose of the amplitudes of $|\psi\rangle$ viewed as a matrix in the left (i, j) and right (α, β) indices, and $\bar{\cdot}$ denotes averaging over the Gaussian ensemble. The operators δ^l_{ij} and $\delta^r_{\alpha\beta}$ project onto the l and r sectors of the left and right subsystems, respectively. That is, $\delta^l_{ij} = 1$ if $i = j$ and the configuration labeled by i is in sector l. With this notation, the reduced density matrix for the left subsystem is $\hat{\rho} = \psi\psi^\dagger$.

The normalization of Eq. (3) is convenient for the diagrammatics below. However, one must appropriately include normalization factors of

$$\mathcal{N} = \overline{\mathrm{Tr}\hat{\rho}} = N\sum_{lr} C_{lr}d_l d'_r \triangleq N(\phi^2 + 2\phi) \tag{4}$$

in the final formulas. Technically, one should sample $|\psi\rangle$ from the Haar measure and ensure the normalization of $\hat{\rho}$. We use the Gaussian measure in the large-N limit since correlations between the numerator and denominator (the normalization) of any moment are suppressed.

The calculation of the ensemble averaged trace moments of the reduced density operator $\overline{\mathrm{Tr}\hat{\rho}^n}$ may be organized diagrammatically using Wick's theorem as follows. (1) Introduce a single solid [dashed] line to represent each left (i, j) [right (α, β)] index contraction.

$$\delta^l_{ij} = \underline{\quad l \quad} \qquad \delta^r_{\alpha\beta} \quad \text{---} r \text{---} \tag{5}$$

Each line carries a "spin" label l (r) which indicates the sector of the left (right) subsystem and which must be

summed over to evaluate the diagram. (2) Introduce vertices for each insertion of ψ or $\psi^\dagger$:

(6)

In $\mathrm{Tr}\hat{\rho}^n$, the ψ and $\psi^\dagger$ factors alternate so these two rules produce a circle of alternating solid and dashed lines. Finally, (3) each Wick pairing is represented by a double line,

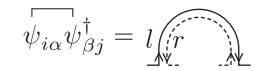

(7)

connecting the tops of the vertices consistent with the arrows and solid or dashed lines. The spin labels carried by the double lines must satisfy the constraint encoded by C.

For example, the second trace moment may be evaluated diagrammatically,

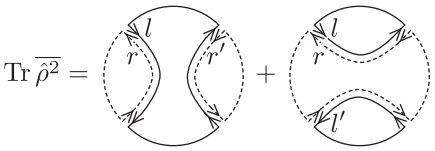

(8)

$$\widehat{=} 2N(\phi^3 + 3\phi^2 + \phi)$$

Each diagram arising in the evaluation of $\mathrm{Tr}\overline{\hat{\rho}^n}$ may be viewed as a surface with a circular boundary [35–40]. The double lines are the internal edges separating faces (loops) while the single lines make up the outer boundary. Since each closed loop contributes a factor of Nd_l or Nd'_r and each double line contributes $1/N$, the N dependence of the diagram is given by the Euler characteristic χ of the surface. Accordingly, the large N limit picks out the planar diagrams with $\chi = 1$. Moreover, the relative fluctuations of any trace moment vanish at large N: the connected correlators $\overline{(\mathrm{Tr}\cdot)(\mathrm{Tr}\cdot)}_c$ have two circular boundaries so that $\chi \leq 0$. The entire sequence of trace moments and corresponding DOS is thus self-averaging at large N.

In general, there are C_n planar diagrams in $\mathrm{Tr}\overline{\hat{\rho}^n}$, each of which contributes a nontrivial polynomial in the relative dimensions. Here, C_n is the nth Catalan number. For the unconstrained case, the polynomial is trivial and $\mathrm{Tr}\overline{\hat{\rho}^n} = NC_n$ correctly reproduces the moments of the MP law.

Entanglement spectrum.—To calculate the density of states (DOS) of $\hat{\rho}$, we turn to the resolvent

$$\hat{G}(z) = \overline{\frac{1}{z - \hat{\rho}}} \tag{9}$$

which, by the Haar symmetry of $|\psi\rangle$, is diagonal and constant in each sector l of the left Hilbert space,

$$\hat{G}(z) = \sum_l \delta^l G_l(z) \triangleq \delta^0 G_0(z) + \delta^1 G_1(z). \tag{10}$$

The diagonal matrix elements $G_l(z)$ determine the mean entanglement DOS associated with the l sector,

$$p_l(x) = \frac{-1}{\pi} \mathrm{Im} G_l(x + i0^+). \tag{11}$$

The distribution p_l is normalized so that $\int dx p_l(x) = 1$; the total DOS takes into account the relative dimension between the sectors:

$$p(x) = \frac{\sum d_l p_l(x)}{\sum d_l} \triangleq \frac{\phi p_0(x) + p_1(x)}{\phi + 1}. \tag{12}$$

In order to correct for the normalization of Eq. (4), we will eventually change variables from x to

$$\epsilon = \frac{N \sum_l d_l}{\mathcal{N}} x \triangleq \frac{\phi + 1}{\phi^2 + 2\phi} x. \tag{13}$$

This scales the eigenvalues of $\hat{\rho}$ such that $\mathrm{Tr}\hat{\rho}$ is the dimension of the left Hilbert space.

To compute the resolvent $\hat{G}(z)$, we expand

$$\hat{G}(z) = \frac{1}{z} \sum_{k=0}^{\infty} \frac{\overline{\hat{\rho}^k}}{z^k} \tag{14}$$

and sum over all planar diagrams generated by the Wick contractions of $\overline{\hat{\rho}^k} = \overline{(\psi\psi^\dagger)^k}$. This is analogous to the moment method typically used in random matrix theory. We rearrange the sum over diagrams to obtain a Dyson series with self-energy relations of the following form,

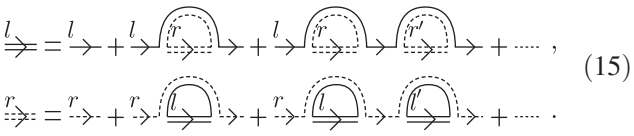

(15)

In these diagrams, the single solid line (bare propagator for left indices) carries an extra $1/z$ compared to the rules described in the previous section.

Resumming the Dyson series we obtain the governing equations,

$$G_l = \frac{1}{z - \Sigma_l}, \qquad \Sigma_l = \sum_r C_{lr} d'_r H_r, \tag{16}$$

$$H_r = \frac{1}{1 - \Sigma'_r}, \qquad \Sigma'_r = \sum_l C_{lr} d_l G_l, \tag{17}$$

where H_r denotes the full propagator for the dashed lines and Σ and Σ' are self-energies. The correct branch of solutions for $G_l(z)$ must be analytic in the upper half plane and decay as $1/z$ in order to correspond to a properly normalized $p_l(x)$.

As a simple check, consider the bipartition in an unconstrained space. Equation (16) reduces to a quadratic equation for $G(z)$ whose solution, $G_{\mathrm{MP}}(z) = (1 - \sqrt{1 - 4/z})/2$, indeed reproduces the MP law, Eq. (1).

Blockaded chain.—For the constraint structure of Eq. (2), some algebra reveals that G_0 satisfies a cubic equation,

$$G_0^3 - \frac{2}{\phi} G_0^2 + \frac{z + \phi - 1}{z\phi^2} G_0 - \frac{1}{z\phi^2} = 0 \tag{18}$$

and that G_1 can be expressed in terms of G_0,

$$\frac{1}{G_1} = \frac{1}{G_0} + \frac{1}{1 - \phi G_0}. \tag{19}$$

The complete solution of these equations exploiting the Vieta formula can be found in the Supplemental Material [34].

The salient features of the resulting entanglement spectra are illustrated in Fig. 1. As a function of the relative dimension ϕ, there are three "entanglement phases," distinguished by the nature of the singularity in the DOS $p(\epsilon)$ as $\epsilon \to 0$. We dub the regime $\phi > 1$ the *MP phase* as $p(\epsilon) \sim \epsilon^{-1/2}$, just like the MP law in Eq. (1). Indeed, for $\phi \to \infty$, the (0,0) sector of the composite Hilbert space dominates the amplitude matrix $\psi_{i\alpha}$ and $p(\epsilon)$ approaches the MP law exactly. At any finite $\phi > 1$, however, $p(\epsilon)$ deviates quantitatively.

For $\phi < 1$, the continuous part of the DOS gaps away from a delta function located at $\epsilon = 0$. The delta function has mass $(1 - \phi)/(1 + \phi)$, which follows from the number of linearly independent columns in a full rank matrix $\psi_{i\alpha}$ with the block structure shown in Fig. 2. Qualitatively similar behavior arises in unconstrained systems when the dimensions of the two subsystems are unequal.

The multicritical point at $\phi = 1$ has no counterpart in unconstrained systems. The DOS exhibits a nontrivial power law $p(\epsilon) \sim \epsilon^{-2/3}$. The multicritical point is realized, for example, by the defect chain in which the Hilbert space is constrained across the single strong central bond.

Figure 3 presents numerical evidence that each of the three entanglement singularities is actually realized by the quasienergy eigenstates of three thermalizing Floquet models in constrained spin chains (see [34] for details of the models). In particular, the quasienergy states of the defect chain readily exhibit the multicritical exponent $p(\epsilon) \sim \epsilon^{-2/3}$.

Entropy corrections.—There is very little information regarding a global random pure state from measurements confined to a subsystem. This can be quantified using the Renyi ($n \neq 1$) and von Neumann ($n = 1$) entanglement entropies,

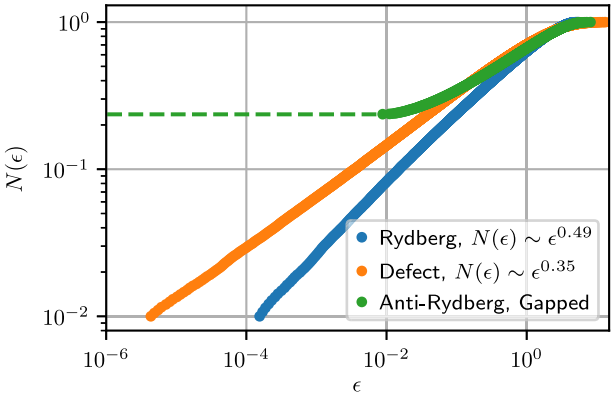

FIG. 3. Integrated DOS $N(\epsilon)$ averaged across all quasienergy states for three local, thermalizing Floquet models on constrained chains. The Rydberg and Defect models show the universal exponents of the MP phase and the multicritical point, respectively. The anti-Rydberg chain lies in the gapped phase, so $N(\epsilon)$ begins at a finite value in the logarithmic plot.

$$S_n(\hat{\rho}) \equiv \frac{1}{1 - n} \ln \frac{\mathrm{Tr}\hat{\rho}^n}{(\mathrm{Tr}\hat{\rho})^n}. \tag{20}$$

A typical random pure state in an unconstrained system has entropy nearly that of the infinite temperature mixed state on the same system. Indeed, Page famously showed that the deviation

$$\Delta S_n = S_n(\hat{\rho}^{T=\infty}) - \overline{S_n(\hat{\rho})} \tag{21}$$

is less than or equal to $1/2$ for $n = 1$ even though S_1 itself is extensive.

We expect modifications to both terms in Eq. (21) for constrained systems because (i) $\hat{\rho}^{T=\infty} \propto \sum_{lr} \delta^l C_{lr} d'_r$ is not the identity operator on the left space, and (ii) the entanglement DOS $p(\epsilon)$ for the random state is different from the MP law. Because of the concentration of measure at large N, the average entropy depends explicitly on $p(\epsilon)$:

$$\overline{S_n(\hat{\rho})} = \ln\left(N \sum d_l\right) + \frac{1}{1 - n} \ln\left(\int d\epsilon p(\epsilon) \epsilon^n\right). \tag{22}$$

For example, the Page correction at $n = 1$ for the Rydberg chain [$\phi = (1 + \sqrt{5})/2$]:

$$\Delta S_1 \approx 0.513595\cdots \tag{23}$$

is larger than the value $1/2$ of the unconstrained chain, violating the Page inequality [34]. The half subsystem has more information regarding the pure global state in the constrained chain than it does in the unconstrained case.

Global symmetries.—Many systems have *diagonal* constraints, which impose a one-to-one relationship between allowed l and r sectors. For example, global S^z conservation constrains the total S^z on the left l and right r to add up

to the total magnetization M. Systems of pinned non-Abelian anyons provide a more exotic example. Net fusion into the vacuum channel constrains left and right fusion sectors to be conjugate [41].

As each (l, r) sector may be viewed as a product space, the total DOS is a linear combination of scaled and re-weighted MP laws:

$$p(x) \propto \sum_l \frac{d_l}{d'_r} p_{\mathrm{MP}}^{(\lambda_l)}\left(\frac{x}{d'_r}\right). \tag{24}$$

Here, $p_{\mathrm{MP}}^{(\lambda)}(x)$ is the unbalanced MP distribution [7], which arises when $\lambda_l = d_l/d'_r$ deviates from 1.

In a spin-1/2 chain with S^z conservation, $\lambda = \binom{L}{M-l}/\binom{L}{l}$ is generically not equal to 1. Direct computation from (24) reproduces the Renyi entropies calculated in [42–45] for globally constrained systems [46].

The balanced case, where all allowed sectors have $d_l = d'_r$, arises for the S^z-conserving chain at $M = 0$ or for symmetric bipartitions of pinned anyons. Although the total DOS $p(x) \neq p_{\mathrm{MP}}(x)$, it lies in the MP phase since the $\epsilon^{-1/2}$ singularity persists. Remarkably, the Page corrections are actually *unmodified* from those of the simple MP law, $\Delta S_n = [1/(n-1)] \ln C_n$.

Discussion.—We have developed a diagrammatic technique to compute the entanglement DOS $p(\epsilon)$ of random pure states in a wide array of constrained systems. This leads to entanglement phases which are classified by the singularity structure of $p(\epsilon)$ at small ϵ. We have focused on bipartitions into equally sized left and right subsystems. For unconstrained systems, it is well known that $p_{\mathrm{MP}}^{(\lambda)}(\epsilon)$ gaps for unbalanced cuts. This extends to constrained systems. Taking $d = \lambda d'$, the MP phase in Fig. 1 may be viewed as a critical boundary at $\lambda = 1$ in the $\phi - \lambda$ plane. It has two natural critical exponents, $p(\epsilon) \sim \epsilon^{-1/2}$ and $\Delta \sim |\lambda - 1|^2$, governing the DOS and gap scaling, respectively. The multicritical point at $\phi = \lambda = 1$ terminates the MP phase with exponents $p(\epsilon) \sim \epsilon^{-2/3}$ and $\Delta \sim (1-\phi)^3$ (on the $\lambda = 1$ boundary). We showed that the multicritical point is realized by the defect chain, a spin-1/2 chain with an infinite penalty for the (1,1) state of the two spins across the central cut.

We do not expect to be able to solve for the DOS for constrained systems with more than two boundary sectors in closed form: the self-consistency equations will be higher than quartic order. Nevertheless, the equations can be analyzed asymptotically at small z in order to extract the entanglement phases and numerically solved to extract $p(\epsilon)$ to any desired precision.

The Page correction ΔS_1 quantifies the information that half of a system has regarding the purity of the global state. Intriguingly, $\Delta S_1(\phi) > 1/2$ for all ϕ; heuristically, the blockade constraint provides more information to the subsystem than is available in the unconstrained case. We conjecture that Page's result is a lower bound to ΔS_1 across all constrained systems.

Entanglement spectra have played an important role in classifying symmetry-protected topological orders in highly excited states in many body localized phases [47–50]. Our results provide the baseline modified entanglement spectrum in the adjacent ETH (eigenstate thermalization hypothesis) phase due to symmetry restrictions.

The authors would like to thank C. Chamon, A. Hamma, P. Krapivsky, A. Polkovnikov and Z. Yang for stimulating discussions. C. R. L. and A. C. acknowledge support from the Sloan Foundation through Sloan Research Fellowships, and from the NSF through Grants No. PHY-1752727 and No. DMR-1752759, respectively. Any opinion, findings, and conclusions or recommendations expressed in this material are those of the authors and do not necessarily reflect the views of the NSF.

[1] H. Li and F. D. M. Haldane, Phys. Rev. Lett. **101**, 010504 (2008).
[2] E. P. Wigner, Ann. Math. **62**, 548 (1955).
[3] F. J. Dyson, J. Math. Phys. (N.Y.) **3**, 140 (1962).
[4] M. L. Mehta, *Random Matrices*, Vol. 142 of Pure and Applied Mathematics, 3rd ed. (Elsevier, 2004).
[5] T. Guhr, A. Müller-Groeling, and H. A. Weidenmüller, Phys. Rep. **299**, 189 (1998).
[6] V. E. Kravtsov, arXiv:0911.0639.
[7] V. A. Marčenko and L. A. Pastur, Math. USSR-Sbornik **1**, 457 (1967).
[8] J. M. Deutsch, Phys. Rev. A **43**, 2046 (1991).
[9] M. Srednicki, Phys. Rev. E **50**, 888 (1994).
[10] M. Rigol, V. Dunjko, and M. Olshanii, Nature (London) **452**, 854 (2008).
[11] S. Goldstein, J. L. Lebowitz, R. Tumulka, and N. Zanghì, Phys. Rev. Lett. **96**, 050403 (2006).
[12] S. Popescu, A. J. Short, and A. Winter, Nat. Phys. **2**, 754 (2006).
[13] L. D'Alessio, Y. Kafri, A. Polkovnikov, and M. Rigol, Adv. Phys. **65**, 239 (2016).
[14] Z.-C. Yang, C. Chamon, A. Hamma, and E. R. Mucciolo, Phys. Rev. Lett. **115**, 267206 (2015).
[15] S. D. Geraedts, N. Regnault, and R. M. Nandkishore, New J. Phys. **19**, 113021 (2017).
[16] D. N. Page, Phys. Rev. Lett. **71**, 1291 (1993).
[17] L. D'Alessio and M. Rigol, Phys. Rev. X **4**, 041048 (2014).
[18] L. Zhang, H. Kim, and D. A. Huse, Phys. Rev. E **91**, 062128 (2015).
[19] D. J. Luitz, N. Laflorencie, and F. Alet, Phys. Rev. B **91**, 081103(R) (2015).
[20] P. Ponte, Z. Papić, F. Huveneers, and D. A. Abanin, Phys. Rev. Lett. **114**, 140401 (2015).
[21] L. Zhang, V. Khemani, and D. A. Huse, Phys. Rev. B **94**, 224202 (2016).
[22] L. Balents, Nature (London) **464**, 199 (2010).
[23] R. Moessner and K. S. Raman, in *Quantum Dimer Models* (Springer Berlin Heidelberg, Berlin, Heidelberg, 2011), pp. 437–479.

[24] A. Feiguin, S. Trebst, A. W. W. Ludwig, M. Troyer, A. Kitaev, Z. Wang, and M. H. Freedman, Phys. Rev. Lett. **98**, 160409 (2007).
[25] C. Gils, E. Ardonne, S. Trebst, A. W. W. Ludwig, M. Troyer, and Z. Wang, Phys. Rev. Lett. **103**, 070401 (2009).
[26] M. Saffman, T. G. Walker, and K. Mølmer, Rev. Mod. Phys. **82**, 2313 (2010).
[27] H. Bernien, S. Schwartz, A. Keesling, H. Levine, A. Omran, H. Pichler, S. Choi, A. S. Zibrov, M. Endres, M. Greiner *et al.*, Nature (London) **551**, 579 (2017).
[28] A. M. Kaufman, M. E. Tai, A. Lukin, M. Rispoli, R. Schittko, P. M. Preiss, and M. Greiner, Science **353**, 794 (2016).
[29] A. Chandran, M. D. Schulz, and F. J. Burnell, Phys. Rev. B **94**, 235122 (2016).
[30] Z. Lan and S. Powell, Phys. Rev. B **96**, 115140 (2017).
[31] C. Chen, F. Burnell, and A. Chandran, Phys. Rev. Lett. **121**, 085701 (2018).
[32] M. Brenes, M. Dalmonte, M. Heyl, and A. Scardicchio, Phys. Rev. Lett. **120**, 030601 (2018).
[33] C. J. Turner, A. A. Michailidis, D. A. Abanin, M. Serbyn, and Z. Papić, Nat. Phys. **14**, 745 (2018).
[34] See Supplemental Material at http://link.aps.org/supplemental/10.1103/PhysRevLett.124.050602 for details.
[35] G. 't Hooft, Nucl. Phys. **B72**, 461 (1974).
[36] E. Brézin and A. Zee, Phys. Rev. E **49**, 2588 (1994).
[37] P. W. Brouwer and C. W. J. Beenakker, J. Math. Phys. **37**, 4904 (1996).
[38] J. Jurkiewicz, G. Lukaszewski, and M. A. Nowak, Acta Phys. Pol. **B39**, 799 (2008).
[39] A. Zee, *Quantum Field Theory in a Nutshell, 2nd Edition (In a Nutshell)* (Princeton University Press, 2010).
[40] S. C. Morampudi and C. R. Laumann, arXiv:1808.08674 [Phys. Rev. B (to be published)].
[41] P. Bonderson, Ph.D. thesis, Caltech, 2007.
[42] T.-C. Lu and T. Grover, Phys. Rev. E **99**, 032111 (2019).
[43] J. R. Garrison and T. Grover, Phys. Rev. X **8**, 021026 (2018).
[44] A. Dymarsky, N. Lashkari, and H. Liu, Phys. Rev. E **97**, 012140 (2018).
[45] L. Vidmar and M. Rigol, Phys. Rev. Lett. **119**, 220603 (2017).
[46] We note that Refs. [42–44] take the Gibbs ensemble to be defined by a subsystem Hamiltonian rather than the partial trace of a global Gibbs state. The page corrections following from our definition remain $O(1)$ for all Renyi indices n.
[47] D. A. Huse, R. Nandkishore, V. Oganesyan, A. Pal, and S. L. Sondhi, Phys. Rev. B **88**, 014206 (2013).
[48] A. Chandran, V. Khemani, C. R. Laumann, and S. L. Sondhi, Phys. Rev. B **89**, 144201 (2014).
[49] Y. Bahri, R. Vosk, E. Altman, and A. Vishwanath, Nat. Commun. **6**, 7341 (2015).
[50] M. Goihl, C. Krumnow, M. Gluza, J. Eisert, and N. Tarantino, SciPost Phys. **6**, 72 (2019).